ACS APPLIED MATERIALS & INTERFACES

Research Article

www.acsami.org

Hexaphenylbenzene-Based Fluorescent Aggregates for Ratiometric Detection of Cyanide Ions at Nanomolar Level: Set−Reset Memorized Sequential Logic Device

Subhamay Pramanik, Vandana Bhalla,* and Manoj Kumar*

Department of Chemistry, UGC Sponsored Centre for Advanced Studies-1, Guru Nanak Dev University, Amritsar-143005, Punjab, India

Supporting Information

ABSTRACT: A hexaphenylbenzene-based receptor **3** has been synthesized that forms a fluorescent spherical aggregate in mixed aqueous media due to its aggregation-induced emission enhancement attributes. These fluorescent spherical aggregates show ratiometric response toward cyanide ions via nucleophilic addition and undergo deaggregation to form smaller nanoaggregates. In addition, the solution-coated paper strips of **3** can detect cyanide ions in the range of ∼2.6 ng/cm^2, thus, providing a simple, portable, and low-cost method for detection of cyanide ions in aqueous media. Receptor **3** also behaves as a set−reset memorized sequential logic circuit with chemical inputs of CN^- ions and trifluoroacetic acid or H^+ (pH ≤ 3).

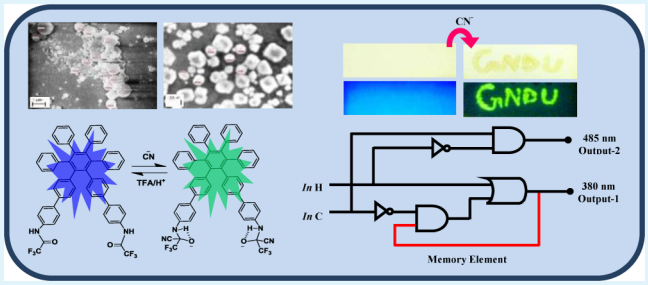

KEYWORDS: *hexaphenylbenzene, AIEE, cyanide, ratiometric, fluorescent nanoaggregates, sequential device*

INTRODUCTION

Among various anions, cyanide is one of the most toxic inorganic anions to living organisms, and consequently, its release into the environment is harmful.[1] Absorption of cyanide through the lungs, gastrointestinal tract, and skin can lead to convulsions, loss of consciousness, and eventually death.[2] Further, the binding of cyanide to the iron species in cytochrome-*c* oxidase reduces the activity of this enzyme and inhibits oxygen utilization by cells.[3] It is known that 0.5−3.5 mg per kg of body weight is lethal for humans.[4] According to the World Health Organization (WHO), water having cyanide concentrations lower than 1.9 μM are acceptable for drinking.[5] Recent studies have shown that the poisonous cyanide concentration in the blood of fire victims is ca. 20 μM.[6] Unfortunately, the use of cyanide ions cannot be avoided due to its widespread applications in various industrial processes, such as gold mining,[7] electroplating, metallurgy, and production of organic chemicals and polymers, e.g., nitriles, nylon, and acrylic plastics.[8] Keeping in view the utility of cyanide ions in day-to-day life, there is a great need for receptors that can selectively detect cyanide ions by simple spectral analysis. In this context, various types of fluorometric[9] and colorimetric[10] CN^- selective receptors have been reported[11−18] based on the mechanism of coordination,[19] hydrogen-bonding interactions,[20,21] nucleophilic addition reactions,[22−26] and metal−cyanide affinity[27−29] (displacement approach). Among various types of chemosensors reported so far, the reaction based chemosensors showing ratiometric response toward cyanide are advantageous due to their high selectivity and sensitivity. Ratiometric responses are attractive because the ratio between the two emission intensities can be used to measure analyte concentration and provide built-in correction for environmental effects and stability under illumination. Thus, reaction based chemosensors showing ratiometric responses toward cyanide ions are highly desirable. However, there are many more reports in the literature about reaction based chemosensors showing ratiometric response toward cyanide ions,[30−32] but most of the reported reaction based chemosensors suffer from several limitations, such as poor selectivity, require high temperature or basic medium, slow response toward cyanide ions,[33,34] high detection limits, risk of releasing HCN,[35] irreversibility (based on reaction), and require an organic environment to function.[36,37] Thus, development of a quick,[38,39] facile, reversible and ratiometric reaction based fluorogenic sensor, which works in aqueous media with low detection limit, is still a challenge.[40,41]

Our research work involves the development of fluorogenic chemosensors for selective detection of different types of analytes.[42−45] Recently, we reported a hexaphenylbenzene (HPB) derivative **1** (Chart 1) appended with β-naphthol moieties that showed aggregation-induced emission enhancement (AIEE) phenomena in mixed aqueous medium to form spherical nanoaggregates.[20] These nanoaggregates undergo further self-assembly to form the modulated nanorods in the

Received: February 12, 2014
Accepted: March 31, 2014
Published: March 31, 2014

   dx.doi.org/10.1021/am500903d | ACS Appl. Mater. Interfaces 2014, 6, 5930−5939

Chart 1. HPB Derivative 1[20]

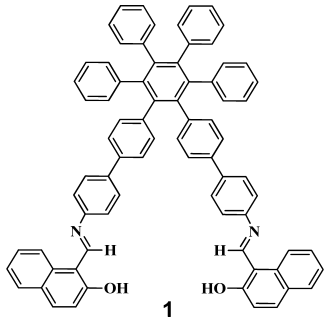

1

presence of cyanide ions.[20] The supramolecular aggregates contain hydroxyl groups on their outer surface on which the cyanide ions are adsorbed through H-bonding interaction, which facilitates the formation of modulated nanorods. In continuation of this work, we are now interested in preparation of a hexaphenylbenzene derivative appended with amide moieties as amides are known to interact with anions through hydrogen bonding between anions and amide −NH groups. On the other hand, amides are also susceptible to nucleophilic attack on carbonyl carbon.[22,46] Keeping this in mind, we designed and synthesized HPB derivative **3** having amide moieties in which the electrophilicity of the carbonyl carbon is enhanced by the presence of a $-CF_3$ group in its vicinity. We believed that HPB derivative **3** would exhibit AIEE[47−49] characteristics due to the presence of a hexaphenylbenzene moiety[20,44] and the aggregation process could be further facilitated due to formation of intermolecular hydrogen bonds (−N−H···O═C−) between adjacent molecules. Further, we envisioned that this intermolecular hydrogen bonding in HPB derivative **3** could be interrupted in the presence of analytes, which may lead to a change in the photophysical properties of supramolecular aggregates. To our pleasure, aggregates of HPB derivative **3** in aqueous medium undergo deaggregation in the presence of CN^- ions and show fast, selective "ratiometric" and "naked eye" response toward cyanide ions. We believe that this is one of the best reaction based ratiometric and colorimetric chemosensors for CN^- ions among all the chemosensors reported in the literature.[50] Furthermore, this is the first report where aggregates of hexaphenylbenzene derivative **3** serve as a ratiometric chemosensor for cyanide ions in aqueous media. In addition, the suitability of **3** for a paper strip assay provides a simple and selective method for the detection of cyanide in aqueous medium at the nanogram level.

Further, on the basis of the fluorescence behavior of receptor **3** with cyanide ions and TFA (H^+), a sequential logic circuit has been designed. Sequential logic circuits are the functions of both past and present inputs, operate via the feedback loop in which one of the outputs of the device acts as input, and are memorized as "memory function". The design of such signaling devices is of great significance as they can perform molecular level logic operations analogous to those executed by their macroscopic analogues.

RESULTS AND DISCUSSION

The reaction of hexaphenylbenzene derivative **2**[20] (0.05 g, 0.07 mmol) with an excess of trifluoroacetic anhydride, in glacial acetic acid (5.0 mL), furnished a brown-colored solid compound **3** (0.045 g, 71% yield),[51] mp > 280 °C (Scheme 1).

The structure of compound **3** was confirmed from its spectroscopic and analytical data (Supporting Information, Figures S19−S22). The ^{1}H NMR spectrum showed a singlet at 10.33 ppm corresponding to −NH, six doublets at 7.68, 7.62, 7.43, 7.17, 7.02, and 6.94 ppm, and one quartet at 7.34 ppm and one multiplet at 6.78−6.86 ppm corresponding to aromatic protons. The ^{13}C NMR spectrum showed a peak at 161.47 ppm due to the carbonyl carbon and a signal at 101.78 ppm corresponding to the $-CF_3$ carbon and peaks at 141.63, 141.55, 141.33, 140.90, 138.36, 137.48, 136.81, 132.95, 132.59, 132.33, 132.26, 132.20, 129.03, 128.91, 127.58, 127.44, 127.37, 126.04, 125.55, and 121.57 ppm corresponding to different types of aromatic carbons. The ESI-MS mass spectrum of compound **3** showed a parent ion peak at m/z = 947.3027 $[M + K]^+$. The IR spectrum of compound **3** showed stretching bands at 1717 cm^{-1} corresponding to the −C═O group and 3403 cm^{-1} corresponding to the −NH group. These spectroscopic data corroborate the structure **3** for this compound.

The UV−vis spectrum of receptor **3** in ethanol exhibits a strong absorption band at 282 nm. On addition of water content up to 80% (volume fraction) to the solution of **3** in ethanol, the intensity of entire absorption spectra is gradually increased with the appearance of a level-off tail in the visible region (400−500 nm) that is attributed to the Mie scattering due to formation of aggregates (Figure 1A). The fluorescence spectrum of compound **3** in ethanol exhibits a weak emission band at 380 nm (Φ = 0.011) when excited at 282 nm. However, with increasing percentage of water fraction up to 80% (volume fraction) to the solution of **3** in ethanol (Figure 1B), a gradual enhancement in the emission intensity and quantum yield (Φ = 0.153) is observed (Supporting Information, Figure S2B).

Further, the increase in fluorescence intensity of compound **3** is also observed with increasing fraction of triethylene glycol (TEG) (Supporting Information, Figure S1). The concentration-dependent fluorescent spectra also show the enhancement in the emission intensity (Supporting Information, Figure

Scheme 1. Synthesis of Hexaphenylbenzene-Based Derivative 3

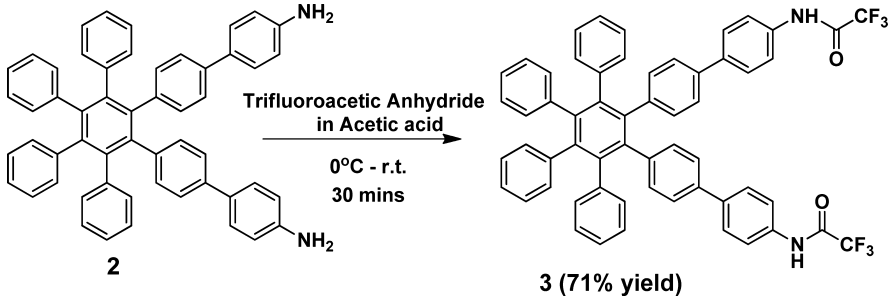

2 3 (71% yield)

dx.doi.org/10.1021/am500903d | ACS Appl. Mater. Interfaces 2014, 6, 5930−5939

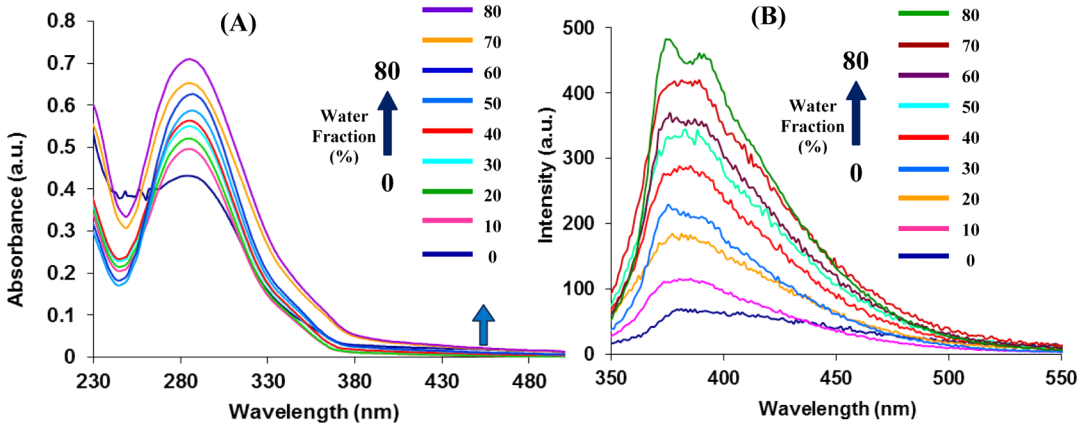

Figure 1. (A) UV−vis spectra of compound **3** (5 μM) showing the variation of absorbance in water/ethanol mixture (0−80% volume fraction of water in ethanol). (B) Change in fluorescence spectra of compound **3** (5 μM) showing the variation of intensity in water/ethanol mixture (0−80% volume fraction of water in ethanol); λ_{ex} = 282 nm.

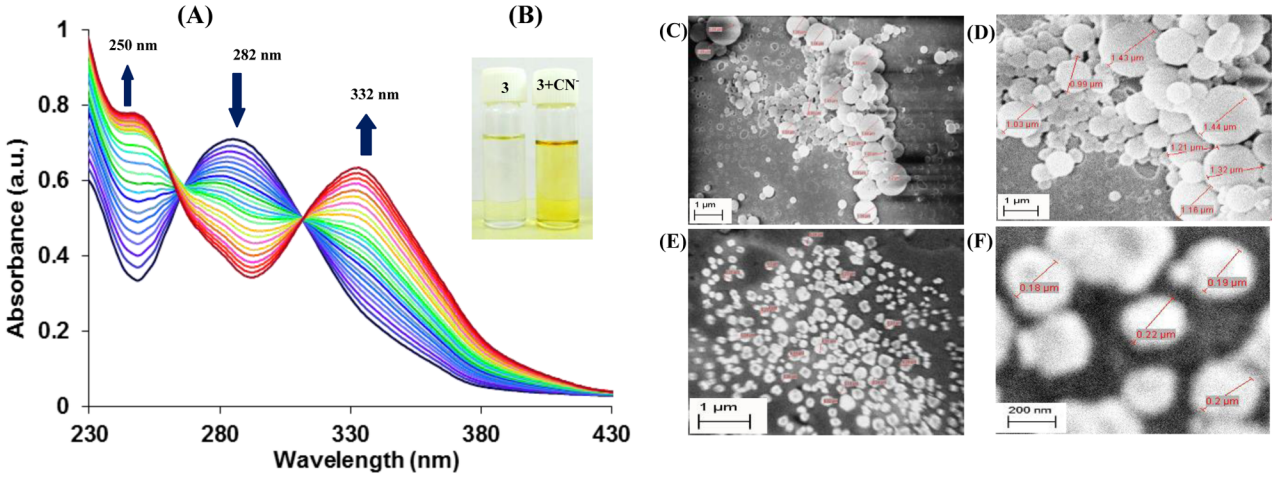

Figure 2. (A) UV−vis spectra of compound **3** (5 μM) showing the response to the CN^- ion (0−250 equiv) in H_2O/EtOH (8:2, v/v) mixture buffered with HEPES; pH = 7.05. (B) Color change of **3** solution in H_2O/EtOH (8:2, v/v) mixture on addition of CN^- ions. Photographs of SEM images (C and D) before and (E and F) after the addition of 250 equiv of CN^- ions in aggregates of **3** in H_2O/EtOH (8:2, v/v) solution.

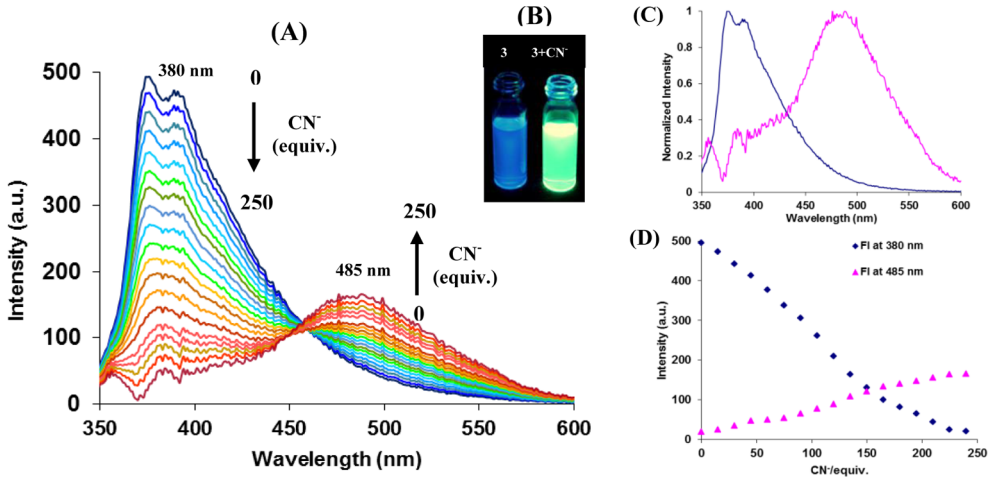

Figure 3. (A) Fluorescence spectra of compound **3** (5 μM) showing the response to the CN^- ion (0−250 equiv) in H_2O/EtOH (8:2, v/v) mixture buffered with HEPES; pH = 7.05, λ_{ex} = 282 nm. (B) Change in fluorescence from blue to green before and after the addition of CN^- ions to **3** in H_2O/EtOH (8:2, v/v) mixture (under 365 nm UV light). (C) The normalized fluorescence intensity at 380 and 485 nm. (D) The change in fluorescence intensity at 380 and 485 nm with the concentration of cyanide ions added.

S2A). We performed concentration-dependent ^{1}H NMR studies that show the downfield shift of 0.23 ppm corresponding to −NH protons and an average upfield shift of 0.10 ppm for HPB protons (Supporting Information, Figure

dx.doi.org/10.1021/am500903d | ACS Appl. Mater. Interfaces 2014, 6, 5930−5939

Scheme 2. Probable Mechanism of Reaction Based Probe 3 with CN^- and TFA

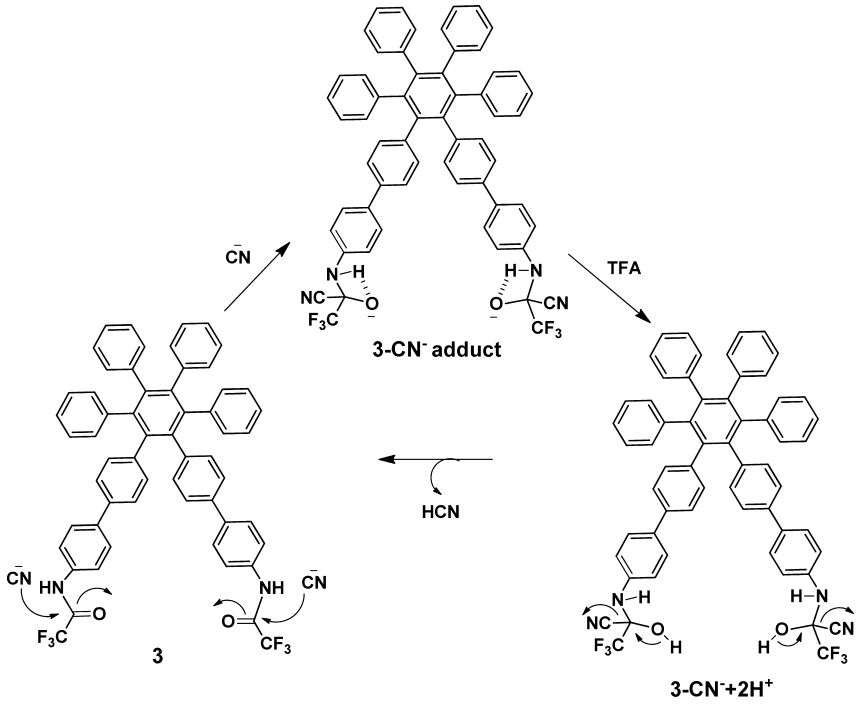

S15). The SEM images (Figure 2C,D) of compound **3** in H_2O/EtOH (8:2, v/v) showed the presence of aggregates of an average particle size of 1.3 μm (Supporting Information, Figure S16A,B), which, hence, clearly support the AIEE characteristics of the molecule.

Since amides are known to interact with anions, we studied the binding ability of HPB derivative **3** toward different anions (CN^-, SCN^-, F^-, Cl^-, Br^-, I^-, NO_3^-, $H_2PO_4^-$, ClO_4^-, CH_3COO^-, and OH^-) using UV−vis and fluorescence spectroscopy. Upon gradual addition of cyanide ions (0−250 equiv) to the solution of **3** (5 μM) in H_2O/EtOH (8:2, v/v), a gradual decrease in absorbance intensity of the band at 282 nm was observed with the appearance of two new absorption bands at 332 and 250 nm along with the formation of two isosbestic points at 265 and 310 nm, respectively (Figure 2A). These results are accompanied by the color change from colorless to yellow (Figure 2B) on addition of CN^- ions to the solution of **3** (5 μM) in H_2O/EtOH (8:2, v/v). Under the same conditions as used above for CN^- ions, we also tested the UV−vis response of compound **3** to other anions, such as SCN^-, F^-, Cl^-, Br^-, I^-, NO_3^-, CH_3COO^-, ClO_4^-, OH^-, and $H_2PO_4^-$, but no change in the absorbance (Supporting Information, Figure S4) behavior was observed in the presence of these anions.

In the fluorescence spectrum, on addition of cyanide ions to the solution of aggregates of HPB derivative **3**, the fluorescence maxima at 380 nm gradually decreased and a new band appeared at 485 nm with an isoemissive point at 455 nm (Figure 3A). These spectral changes are accompanied by the color change of the solution of **3** from blue to green within 5 min of mixing cyanide ions (365 nm UV light, Figure 3B) in a H_2O/EtOH (8:2, v/v) mixture. The fluorescence quantum yield of the **3**-CN^- adducts was calculated to be 0.14 (at 485 nm). Further, by considering the change in fluorescence intensity at 485 nm (I_{485}) and at 380 nm (I_{380}), a 5.5-fold (I_{485}/I_{380}) emission enhancement at 485 nm was observed in the case of the **3**-CN^- adduct (Scheme 2). We also carried out the fluorescence studies of compound **3** in the molecular state with CN^- ions in pure ethanol, but the fluorescence (I_{485}/I_{380}) enhancement was only 2-fold (Supporting Information, Figure S5). Therefore, we performed all the studies of compound **3** in the H_2O/EtOH (8:2, v/v) solvent system.

Further, we also studied the effect of pH on the fluorescence behavior of the **3**-CN^- adduct; the original fluorescence and UV−vis spectra were restored on the addition of trifluoroacetic acid (TFA) (Supporting Information, Figure S3A,B).[19] Furthermore, after the addition of 5 equiv of TFA to the **3**+CN^- mixture in THF-d_8/D_2O (2:8), the −N-H proton reappears at 10.34 ppm with an average downfield shift of 0.22 ppm for all aromatic protons and a new signal appeared at 5.22 ppm corresponding to HCN released in the reaction medium (Supporting Information, Figure S11). These results show the reversibility of the probe in strongly acidic conditions (pH $\leq$ 3) (Scheme 2) (Supporting Information, Figure S3C). The ratiometric response of derivative **3** toward CN^- ions was studied by a fluorescence quenching efficiency plot,[52] which is linear with the increase in concentration of CN^- ions up to 150 equiv with a Stern−Volmer constant (K_{sv}) of 7.8464×10^3 M^{-1} (Supporting Information, Figure S8). The detection limit[53] of CN^- using compound **3** as a fluorescence sensor has been found to be 11 nM[53] (Supporting Information, Figure S9). This detection limit is better than the detection limit of cyanide sensors reported in the literature.[50] Further, the detection limit of TFA for the compound **3**+CN^- adduct has been found to be 95 nM[53] (Supporting Information, Figure S10).

The selectivity of CN^- ions over other anions, in particular fluoride, is important because most of the chemosensors reported for cyanide ions suffer from interference from other anions, especially fluoride ions.[54,55] Under the same conditions as used above for CN^- ions, we also tested the fluorescence response of compound **3** to other anions, such as SCN^-, F^-, Cl^-, Br^-, I^-, NO_3^-, OH^-, CH_3COO^-, ClO_4^-, and $H_2PO_4^-$, but no significant change in emission (Figure 4A, series a) behavior

dx.doi.org/10.1021/am500903d | ACS Appl. Mater. Interfaces 2014, 6, 5930−5939

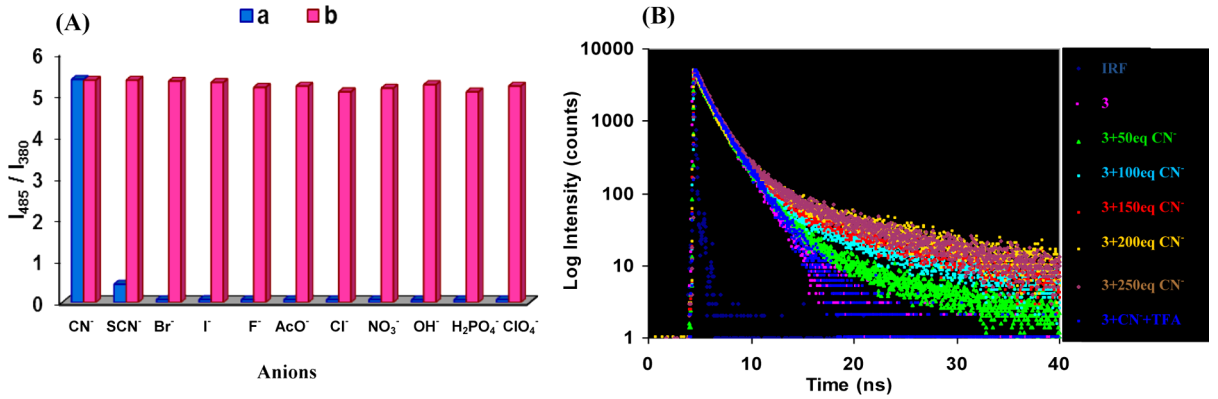

Figure 4. (A) Fluorescence response of **3** (5.0 μM) to various anions (250 equiv) in H_2O/EtOH (8:2, v/v) mixture buffered with HEPES; pH = 7.05; λ_{ex} = 282 nm. Bars represent the emission intensity ratio (I_{485}/I_{380}) (I_{380} = initial fluorescence intensity at 380 nm; I_{485} = final fluorescence intensity at 485 nm after the addition of anions). (a) Blue bars represent selectivity (I_{485}/I_{380}) of **3** upon addition of different anions. (b) Red bars represent competitive selectivity of receptor **3** toward CN^- ions (250 equiv) in the presence of other anions (500 equiv). (B) Exponential fluorescence decays of **3** on addition of CN^- ions measured at 485 nm. Spectra were acquired in H_2O/EtOH (8:2, v/v) mixture buffered with HEPES; pH = 7.05; λ_{ex} = 375 nm.

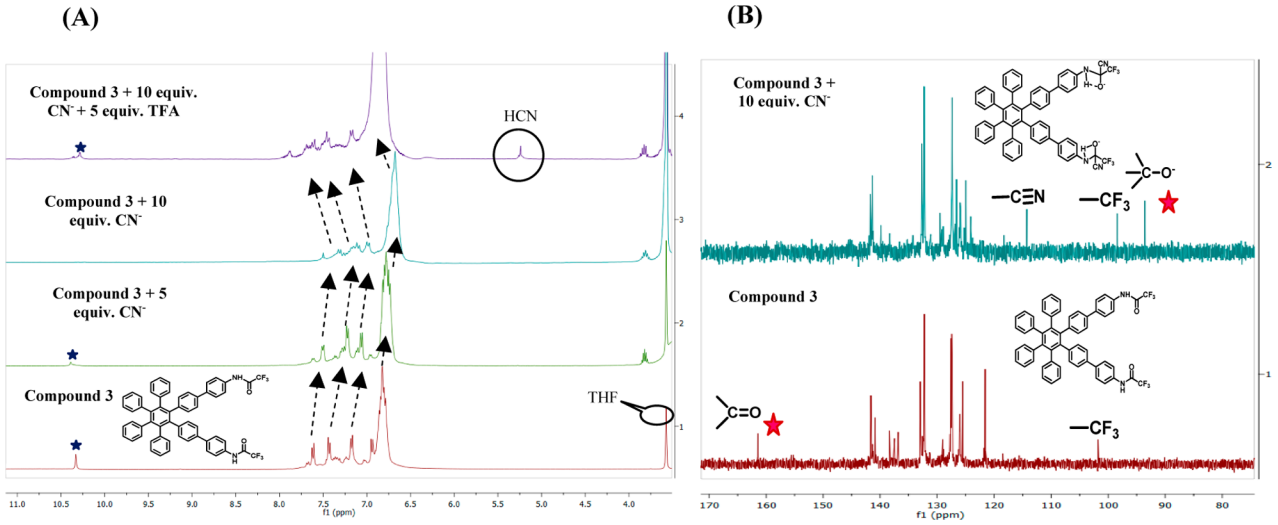

Figure 5. (A) ^{1}H NMR titration of compound **3** with CN^- ions and TFA in THF-d_8/D_2O (2:8). (B) ^{13}C NMR titration of compound **3** with CN^- ions in THF-d_8.

was observed in the presence of these anions. Further, to check the practical applicability of aggregates of **3** as a CN^- sensor, we carried out competitive experiments in the presence of 250 equiv of CN^- in the presence of other anions at 500 equiv; no significant variation in the fluorescence intensity was observed (Figure 4A, series b). Aggregates of **3** can also detect cyanide ions in blood serum containing CN^- ions (Supporting Information, Figure S6) and real water samples, including tap water (Supporting Information, Figure S7A), local ground water (Supporting Information, Figure S7B), and boiled water spiked with the solution of sodium cyanide.

The interaction between anions and derivative **3** has also been studied by the time-resolved fluorescence spectroscopy (Figure 4B).[56] In the absence of anions, derivative **3** exhibits a single-exponential lifetime (τ = 1.46 ns) in H_2O/EtOH (8:2, v/v), whereas, in the presence of cyanide ions, the fluorescence decay of derivative **3** is bi-exponential. This suggests the formation of two distinct species, consisting of the anion bound **3**-CN^- adduct form (τ_1 = 1.91 ns) and free derivative **3** (τ_2 = 0.37 ns). Further, in addition of cyanide ions, the shorter component amplitude gradually decreases (τ_2 = 0.15 ns) and the new longer component amplitude increases (τ_1 = 2.54 ns). On further addition of TFA to the **3**-CN^- adduct, the decay curve revived with a single-exponential lifetime (τ = 1. 39 ns).

The recognition ability of **3** toward various anions (SCN^-, F^-, Cl^-, Br^-, I^-, CN^-, NO_3^-, CH_3COO^-, ClO_4^-, and $H_2PO_4^-$) in the form of their corresponding tetrabutylammonium salts (TBA^+) was also investigated by cyclic voltammetry (CV) in CH_2Cl_2:CH_3CN (1:1) solution containing 0.1 M tetrabutylammonium hexafluorophosphate ($TBAPF_6$) as a supporting electrolyte[57,58] (Supporting Information, Figure S13). The free receptor **3** shows a reversible one-electron redox wave with a half-wave potential ($E_{1/2}$) value of ∼−94 mV. Upon addition of 5.0 equiv of CN^- ions to the solution of **3**, a cathodic shift ($\Delta E_{1/2}$) of ∼−48 mV was observed due to the interaction between cyanide and **3**.[59] In the presence of CN^- ions, due to transfer of electron density from anion to the receptor **3**, the HOMO energy level of the **3**-CN^- adduct is increased and the LUMO energy level is decreased, therefore, narrowing the HOMO−LUMO energy gap from 3.4 to 3.02 V. This narrowing down of the HOMO−LUMO energy gap is

dx.doi.org/10.1021/am500903d | ACS Appl. Mater. Interfaces 2014, 6, 5930−5939

Scheme 3. Probable Schematic Presentation of 3-CN^- Adduct Formation

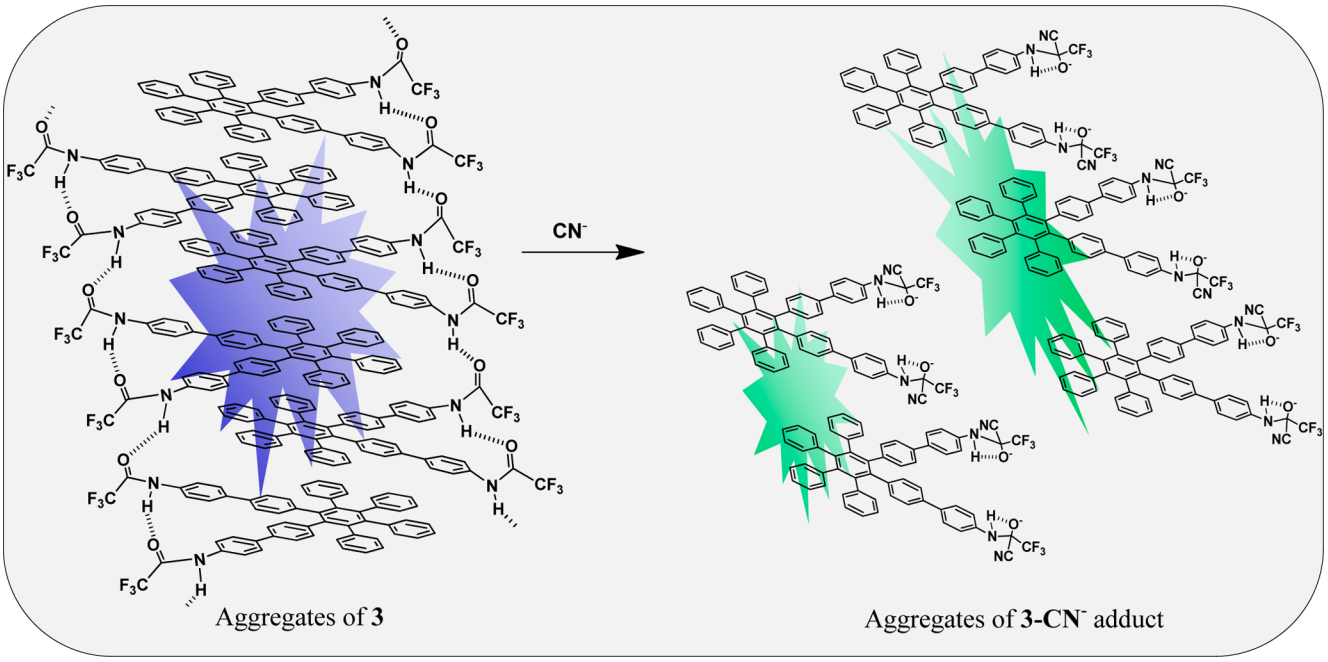

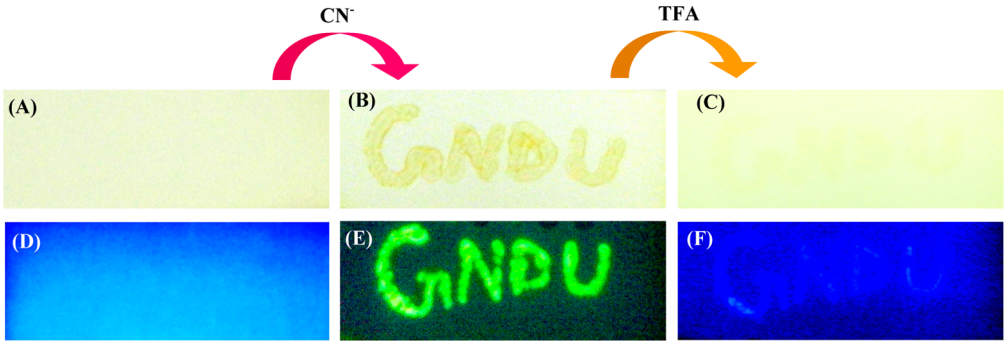

Figure 6. (A–C) Images showing the naked eye color change and (D–F) images showing the fluorescence change under the UV lamp at 365 nm of paper strips coated with chemosensor **3** in response to CN^- ions (10^{-3} M) and TFA (10^{-3} M).

responsible for the large Stokes shift observed in the emission spectrum.[22]

We also carried out ^{1}H NMR, ^{13}C NMR, FT-IR, and ESI-MS studies to get insight into the binding interactions between CN^- ions and **3** (Figure 5). The signal corresponding to the −N-H proton at 10.33 ppm gradually disappeared, and an average upfield shift of 0.21 ppm was observed corresponding to all aromatic protons (Supporting Information, Figure S11) in the ^{1}H NMR spectrum on addition of 10 equiv of CN^- ions to the solution of receptor **3** in THF-d_8/D_2O (2:8).[20] In the ^{13}C NMR spectrum (Figure 5B) of **3** in the presence of CN^- ions, the signal at 161.47 ppm corresponding to the carbonyl carbon disappeared with the appearance of two new signals at 114.58 and at 92.67 ppm corresponding to −CN and −C-O^- carbons and a signal corresponding to the $-CF_3$ carbon shifted slightly upfield from 101.78 to 98.84 ppm (Supporting Information, Figure S12).[60] In the FT-IR spectrum, after the addition of CN^- ions to compound **3**, the peak corresponding to the −C═O group at 1717 cm^{-1} disappeared and two new bands appeared observed at 2156.48 and 1279 cm^{-1} corresponding to −CN and −C-O^- moieties, respectively. Further, the band corresponding to the −N-H group shifted from 3403 to 3223 cm^{-1} due to hydrogen bonding with the electronegative oxygen atom (Supporting Information, Figure S23). The ESI/MS spectrum of the **3**-CN^- adduct shows a molecular ion peak at 512.576 corresponding to the $[M + 2CN + 2H + Na + K]^{2+}$ complex (Supporting Information, Figure S24).

These spectroscopic studies suggest the nucleophilic addition of CN^- ion to the carbonyl group, which leads to disruption of closely packed aggregates, thus, resulting in fluorescence and UV–vis spectral changes. This inference is supported by the SEM and powder X-ray diffraction (XRD) studies. The self-aggregation of derivative **3** was modulated in the presence of CN^- ions. The deaggregation behavior on addition of CN^- ions in receptor **3** can also be explained by the XRD analysis. The powder XRD analysis of derivative **3** displays a broad halo peak at 2θ = 20.8° with a d spacing of 4.27 Å, indicating π–π stacking within the molecules[61−64] (Supporting Information, Figure S14). The SEM images of compound **3** in H_2O/EtOH (8:2, v/v) showed the presence of aggregates of an average particle size of 1.3 μm (Supporting Information, Figure S16A,B). The concentration-dependent ^{1}H NMR spectra show the downfield shift of 0.25 ppm (corresponding to −NH protons) and an average upfield shift of 0.10 ppm for

dx.doi.org/10.1021/am500903d | ACS Appl. Mater. Interfaces 2014, 6, 5930–5939

Table 1

Sr. No.	*In* C	*In* H	380 nm Output-1	485 nm Output-2
1	0	0	1	0
2	1	0	0	1
3	0	1	1	0
4	1(1st)	1(2nd)	1	0
5	1(2nd)	1(1st)	0	1

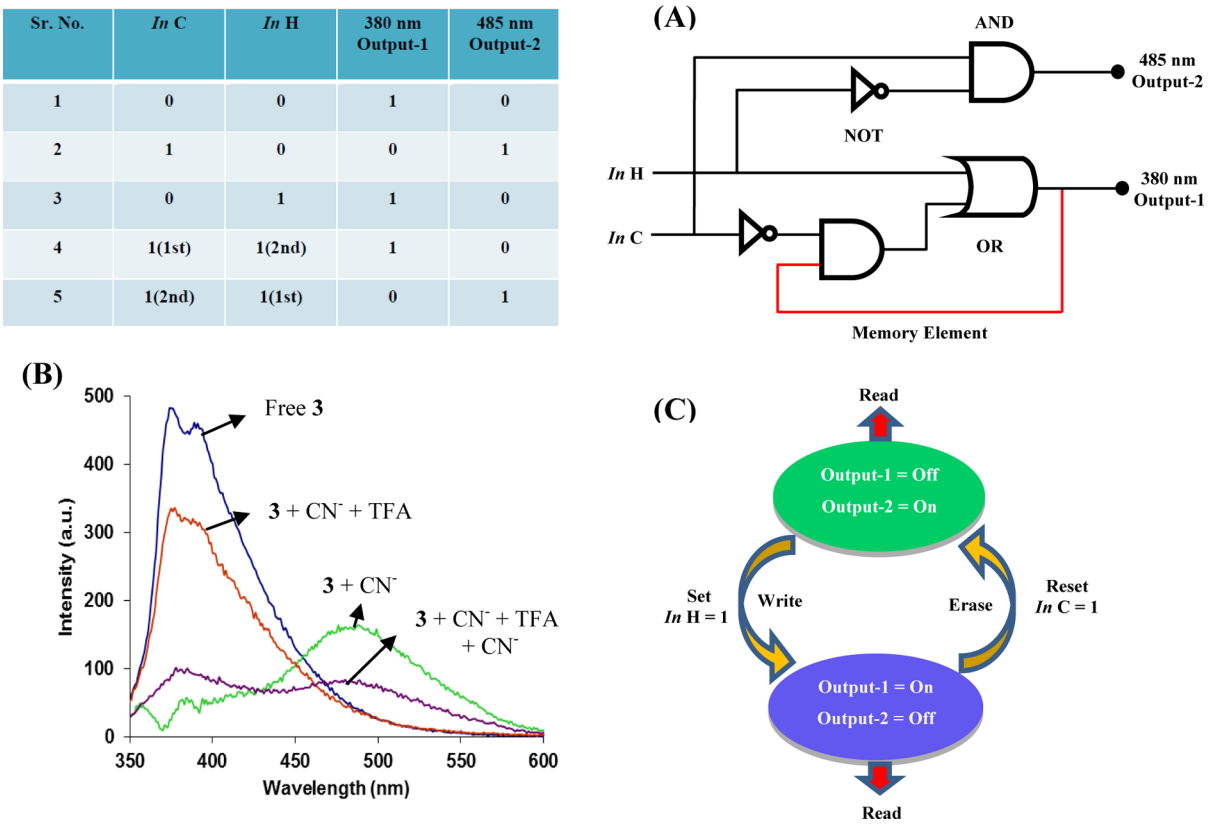

Figure 7. Table 1 is the Truth Table for sequential logic circuit A, where 0 = Off and 1 = On signals. (A) Sequential logic circuit displaying memory units with two inputs (In C and In H) and two outputs (380 and 485 nm). (B) Reversibility of fluorescence spectrum of **3** (5 μM) in the presence of CN^- ions and TFA in H_2O/EtOH (8:2, v/v); λ_{ex} = 282 nm. (C) Schematic representation of the reversible logic operations for memory element possessing "write−read−erase−read" functions.

HPB protons (Supporting Information, Figure S15). These results suggest the presence of $\pi-\pi$ stacking within the derivative **3** in which the molecules are stacked together and amide groups are involved in H-bonding on the surfaces of the aggregates (Scheme 3).[65] On the other hand, the XRD analysis of the **3**-CN^- adduct shows a broad peak at 2θ = 9.7° with a higher d spacing value of 9.1 Å, thus, indicating the loosely arranged molecules. In the presence of CN^- ions, the −NH hydrogen are no longer free for intermolecular H-bonding, showing the disruption of closely packed aggregates to form discrete smaller aggregates (Scheme 3). The SEM images of the **3**-CN^- adduct in H_2O/EtOH (8:2) also show the disruption of closely packed aggregates to form dispersed smaller nano-aggregates (Figure 2E,F) of an average particle size of 200 nm (Supporting Information, Figure S16C,D). The dynamic light scattering (DLS)[49] studies clearly show that, in the presence of CN^- ions, the closely packed aggregates (average diameter of particles = 1.3 μm) are deaggregated to smaller aggregates (average diameter of particles = 200 nm) (Supporting Information, Figure S17). These smaller aggregates show the emission maxima at 485 nm in the fluorescence spectrum. The smaller-sized aggregates are known to emit strongly in the fluorescence spectrum.[66]

We also prepared paper strips by dip-coating a solution of **3** on Whatman filter paper, followed by drying the strips under vacuum. A solution containing Bu_4NCN in H_2O/EtOH (8:2) (10^{-3} M) was sprayed onto the strip by writing "GNDU", and the solvent was evaporated in air. A green fluorescent image with yellow spots appeared on the regions exposed to cyanide ions (Figure 6). For erasing, an ethanol solution of TFA (10^{-3} M) was sprayed onto the strip, the green fluorescent cyanide image disappeared, and the blue fluorescence revived in the cyanide exposed area. We performed the paper strip test in an aqueous solution of cyanide ions. Green fluorescent spots of different concentrations were formed, which show that the regulation of the stimulating behavior of **3** is practically applicable by varying the concentration of CN^- even up to the level of 10^{-6} M (Supporting Information, Figure S18). Further, when a 10 μL volume of 1×10^{-6} M CN^- solution is spotted on the filter paper strips covering an area of 1 cm^2, ~2.6 ng of CN^-, a detection limit of ~2.6 ng/cm^2 is obtained.[67] This means **3** can detect cyanide in a pure water sample at very low concentration, which makes derivative **3** a powerful tool for the detection of cyanide in practical applications.

Recently, the development of sequential logic devices involving the alteration of chemically encrypted information into fluorescent signals has emerged as an active research area of unconventional computing.[68,69] Sequential logic circuits[70] are essential for the realization of memory devices capable of storing information and operating through the feedback loop where one of the outputs of the device functions as the input and is memorized as "'memory element'". Thus, depending upon the different chemical inputs (CN^- and TFA/H^+) and fluorescent signals as outputs (λ_{emis} = 380 and 485 nm), sequential logic circuits are constructed. The two chemical inputs CN^- and TFA/H^+ (pH ≤ 3) are designated as In C and

In H, respectively. The threshold values of fluorescence intensities specified at Output-1 (380 nm) and Output-2 (485 nm) are 150 and 90, respectively. Fluorescence intensities higher than the threshold values are assigned as "1" and intensities lower than the threshold values are assigned as "0", corresponding to the "on" and "off" states of the readout signals, respectively. First, we constructed a logic circuit with two inputs (In C and In H) and two outputs (Figure 7A) measured as the fluorescence emissions at 380 nm (Output-1) and 485 nm (Output-2). The truth table (Figure 7, Table 1) reveals various combinations of inputs for "Output-1" and the sequential logic circuit of "Output-1" emission representing the set/reset element that corresponds to the memory device. The sequential logic operations are presented by two inputs: reset (In C) and set (In H) as a function of the memory element (Figure 7C). The reversible and reconfigurable sequences of set/reset logic operations in a feedback loop demonstrate the memory feature with "write−read−erase−read" functions (Figure 7C) through the output signals at 485 and 380 nm. The reset input (In C = 1) results in the fluorescence off at 380 nm, and this encoded information is "read" out in the system as "erased" and saved as "Output-1 = 0" and "Output-2 = 1". The stored information was "written" by the set input (In H = 1) with the fluorescence on at 380 nm and off at 485 nm, and the system writes and saves "Output-1 = 1" and "Output-2 = 0". Further, the write−erase cycles were performed on receptor **3** through "on−off" fluorescence intensity (at 485 and 380 nm) with good rewritable characteristics as well as visual fluorescence changes by adding CN^- and TFA/H^+ in alternate sequence (Figure 7B).

CONCLUSION

In conclusion, we designed and synthesized an AIEE-active HPB-based receptor **3** for selective detection of cyanide ion in an aqueous medium. A unique colorimetric and ratiometric fluorescent response to cyanide is realized through the formation of the **3**-CN^- adduct via nucleophilic addition of CN^- ions to the highly electron-deficient amide moiety in an aqueous environment. The ∼2.6 ng/cm^2 detection level with high sensitivity achieved by using disposable filter paper based test strips provides a simple and low-cost protocol for the on-site instant detection of cyanide ions in aqueous phase. Further, aggregates of **3** behave as a reversible reaction based system for the ratiometric detection of CN^- ions and TFA/H^+. In addition, these aggregates mimic the functions of a set−reset memorized sequential logic circuit with inputs of CN^- and TFA/H^+ ions (pH ≤ 3).

EXPERIMENTAL SECTION

Materials and Reagents. All reagents were purchased from Aldrich and were used without further purification. THF was dried over sodium and benzophenone as an indicator. UV−vis studies were performed in THF, absolute ethanol, distilled water, and HEPES buffer (0.05 M) (pH = 7.05).

Blood Serum. A real blood sample of a medically fit person was used for the experiment, and all physiological conditions were maintained. The blood serum was isolated by centrifugation of the fresh blood sample of a healthy volunteer after fasting at 4000 rpm for 20 min at 4°C. The stock solution of blood serum was prepared by dissolving 100 μL of serum in 1 mL of a solution of HEPES buffer (0.05 M) at pH = 7.05.

Instrumentation. UV−vis spectra were recorded on a SHIMADZU UV-2450 spectrophotometer, with a quartz cuvette (path length: 1 cm). The cell holder was thermostated at 25°C. The fluorescence spectra were recorded with a SHIMADZU-5301 PC spectrofluorimeter. UV−vis spectra were recorded on a Shimadzu UV-2450PC spectrophotometer with a quartz cuvette (path length: 1 cm). The cell holder was thermostated at 25 °C. The scanning electron microscope (SEM) images were obtained with a field emission scanning electron microscope (SEM JEOL JSM-6610LV). The FT-IR spectra were recorded with a VARIAN 660 IR Spectrometer. The dynamic light scattering (DLS) data were recorded with a Malvern Instruments Nano-ZS. The time-resolved fluorescence spectra were recorded with a HORIBA time-resolved fluorescence spectrometer. ^1H and ^{13}C were recorded on a BRUKER-AVANCE-II FT-NMR-AL400 MHz spectrophotometer using $CDCl_3$, THF-d_8, D_2O as solvent, and tetramethylsilane, $SiMe_4$, as internal standards. Data are reported as follows: chemical shifts in ppm, multiplicity (s = singlet, br = broad signal, d = doublet, t = triplet, m = multiplet), coupling constants J (Hz), integration, and interpretation. Silica gel 60 (60−120 mesh) was used for column chromatography.

Quantum Yield Calculations. Fluorescence quantum yield was determined by using an optically matching solution of diphenylanthracene (Φ_{fr} = 0.90 in cyclohexane) as standard at an excitation wavelength of 373 nm, and quantum yield is calculated using the equation

$$\Phi_{fs} = \Phi_{fr} \times \frac{1 - 10^{-A_r L_r}}{1 - 10^{-A_s L_s}} \times \frac{N_s^2}{N_r^2} \times \frac{D_s}{D_r}$$

Φ_{fs} and Φ_{fr} are the radiative quantum yields of sample and the reference, respectively, A_s and A_r are the absorbance of the sample and the reference, respectively, and D_s and D_r are the respective areas of emission for sample and reference. L_s and L_r are the lengths of the absorption cells of sample and reference, respectively. N_s and N_r are the refractive indices of the sample and reference solutions (pure solvents were assumed, respectively).

UV−vis and Fluorescence Titrations. The concentration of HEPES buffer (pH = 7.05) is 0.05 M. For each experiment, we have taken 3 mL of a solution that contains a solution of derivative **3** in 15 μL of THF diluted with 585 μL of EtOH and 2.4 mL of HEPES buffer (0.05 M, pH = 7.05). UV−vis and fluorescence titrations were performed with 5.0 μM solutions of ligand (15 μL of THF is used to dissolve) in H_2O/EtOH (8:2, v/v). Typically, aliquots of freshly prepared standard solutions (10^{-1} M to 10^{-3} M) of *tert-butyl ammonium salt* ($^tBu_4N^+X^-$), where X = CN^-, F^-, Cl^-, Br^-, I^-, NO_3^-, CH_3COO^-, ClO_4^-, and $H_2PO_4^-$, are used, and trifluoroacetic acid (TFA) in EtOH and freshly prepared standard solutions (10^{-1} M to 10^{-3} M) of metal perchlorates [$M(ClO_4)x$; M = Zn^{2+}, Hg^{2+}, Cu^{2+}, Fe^{2+}, Fe^{3+}, Co^{2+}, Pb^{2+}, Ni^{2+}, Cd^{2+}, Ag^+, Ba^{2+}, Mg^{2+}, K^+, and Na^+; x = 1−2] in EtOH were added to record the UV−vis and fluorescence spectra. In titration experiments, each time, a 3 mL solution of compound was filled in a quartz cuvette (path length: 1 cm) and spectra were recorded.

Synthesis of HPB Derivative 3. To a solution of hexaphenylbenzene-based derivative **2**[20] (0.05 g, 0.07 mmol) in glacial acetic acid (5.0 mL) was added an excess of trifluoroacetic anhydride, in ice-cold conditions, and the resulting reaction mixture was stirred at room temperature for 1 h. The reaction mixture was then poured into ice-cold water for precipitation.[51] The brown-colored solid was filtered and washed with water to furnished compound **3** (0.045 g, 71% yield) mp. > 280 °C (Scheme 1). The structure of compound **3** was confirmed from its spectroscopic and analytical data (Supporting Information, Figures S19−S22). ^1H NMR (400 MHz, THF-d_8): δ = 10.33 (s, 2H, −NH), 7.68 (d, J = 8, 2H, ArH), 7.62 (d, J = 8, 4H, ArH), 7.43 (d, J = 8, 4H, ArH), 7.34 (q, J = 9.2, 2H, ArH) , 7.17 (d, J = 8, 6H, ArH), 7.02 (d, J = 8, 2H, ArH), 6.94 (d, J = 8, 4H, ArH), 6.78-6.86 (m, 12H, ArH). ^{13}C NMR (THF-d_8, 100 MHz): δ = 161.47, 141.63, 141.55, 141.33, 140.90, 138.36, 137.48, 136.81, 132.95, 132.59, 132.33, 132.26, 132.20, 129.03, 128.91, 127.58, 127.44, 127.37, 126.04, 125.55, 121.57, 101.78. ESI-MS mass spectrum of compound **3** showed a parent ion peak, m/z = 947.3027 $[M + K]^+$. The IR spectrum of compound **3** showed stretching bands at 1717 cm^{-1}

corresponding to the −C═O group and 3403 cm^{-1} corresponding to the −NH group.

■ ASSOCIATED CONTENT

Supporting Information

The contents of the Supporing Information include ^{1}H, ^{13}C, mass spectra, and IR spectrum of compound **3**; UV−vis and fluorescence studies; detection limits; SEM images; powder XRD analysis; DLS studies, cyclic voltammogram of **3**; paper strips; and table of comparison of present paper with previous reports. This material is available free of charge via the Internet at http://pubs.acs.org.

■ AUTHOR INFORMATION

Corresponding Authors

*E-mail: mksharmaa@yahoo.co.in (M.K.).
*E-mail: vanmanan@yahoo.co.in (V.B.). Tel.: 91182258802-09, ext. 3202, 3205.

Notes

The authors declare no competing financial interest.

■ ACKNOWLEDGMENTS

M.K. is highly thankful to DST (ref no. SR/S1/OC-69/2012) and V.B. is highly thankful to CSIR (ref. no. 02(0083)/12/EMR-II for financial support. S.P. is thankful to UGC (New Delhi) for a Senior Research Fellowship. We are thankful to UGC (New Delhi, India) for the "University with Potential for Excellence" (UPE) project.

■ REFERENCES

(1) Beer, P. D.; Gale, P. A. Anion Recognition and Sensing: The State of the Art and Future Perspectives. *Angew. Chem., Int. Ed.* **2001**, *40*, 486−516.
(2) Baskin, S. I.; Brewer, T. G. In *Medical Aspects of Chemical and Biological Warfare*; Sidell, F., Takafuji, E. T., Franz, D. R., Eds.; TMM Publications: Washington, DC, 1997; Chapter 10, pp 271−286.
(3) Vennesland, B.; Comm, E. E.; Knownles, C. J.; Westly, J.; Wissing, F. *Cyanide in Biology*; Academic Press: London, 1981.
(4) Kaim, W.; Schwederski, B. *Bioinorganic Chemistry: Inorganic Elements in the Chemistry of Life*; John Wiley & Sons Ltd.: Chichester, England, 1991; p 208.
(5) *Guidelines for Drinking-Water Quality*; World Health Organization: Geneva, Switzerland, 1996.
(6) Ishii, A.; Seno, H.; Suzuki, K. W.; Suzuki, O.; Kumazawa, T. Determination of Cyanide in Whole Blood by Capillary Gas Chromatography with Cryogenic Oven Trapping. *Anal. Chem.* **1998**, *70*, 4873−4876.
(7) Miller, G. C.; Pritsos, C. A. Cyanide: Social, Industrial, and Economic Aspects. In *Proceedings of the TMS Annual Meeting*; TMS: Warrendale, PA, 2001; pp 73−81.
(8) Elvers, B. *Ullmann's Encyclopedia of Industrial Chemistry*, 6th ed; Wiley-VCH: New York, 1999.
(9) Anzenbacher, P.; Tyson, D. S.; Jursíkov, K.; Castellano, F. N. Luminescence Lifetime Based Sensor for Cyanide and Related Anions. *J. Am. Chem. Soc.* **2002**, *124*, 6232−6233.
(10) Miyaji, H.; Sessler, J. L. Off-the-Shelf Colorimetric Anion Sensors. *Angew. Chem., Int. Ed.* **2001**, *40*, 154−157.
(11) Chung, S.; Nam, S.; Lim, J.; Park, S.; Yoon, J. A Highly Selective Cyanide Sensing in Water via Fluorescence Change and Its Application to in Vivo Imaging. *Chem. Commun.* **2009**, 2866−2868.
(12) Robbins, T. F.; Qian, H.; Su, X.; Hughes, R. P.; Aprahamian, I. Cyanide Detection Using a Triazolopyridinium Salt. *Org. Lett.* **2013**, *15*, 2386−2389.
(13) Jackson, R.; Oda, R. P.; Bhandari, R. K.; Mahon, S. B.; Brenner, M.; Rockwood, G. A.; Logue, B. A. Development of a Fluorescence Based Sensor for Rapid Diagnosis of Cyanide Exposure. *Anal. Chem.* **2014**, *86*, 1845−1852.
(14) Shi, B. B.; Zhang, P.; Wei, T. B.; Yao, H.; Lin, Q.; Zhang, Y. M. Highly Selective Fluorescent Sensing for CN^- in Water : Utilization of the Supramolecular Self-Assembly. *Chem. Commun.* **2013**, *49*, 7812−7814.
(15) Maldonado, C. R.; Varela, A. T.; Jones, A. C.; Rivas, J. C. M. A Turn-On Fluorescence Sensor for Cyanide from Mechanochemical Reactions between Quantum Dots and Copper Complexes. *Chem. Commun.* **2011**, *47*, 11700−11702.
(16) Ren, J.; Zhu, W.; Tian, H. A Highly Sensitive and Selective Chemosensor for Cyanide. *Talanta* **2008**, *75*, 760−764.
(17) Xie, Y.; Ding, Y.; Li, X.; Wang, C.; Hill, J. P.; Ariga, K.; Zhang, W.; Zhu, W. Selective, Sensitive and Reversible "Turn-On" Fluorescent Cyanide Probes Based on 2,20-Dipyridylaminoanthracene−Cu^{2+} Ensembles. *Chem. Commun.* **2012**, *48*, 11513−11515.
(18) Peng, L.; Wang, M.; Zhang, G.; Zhang, D.; Zhu, D. A Fluorescence Turn-on Detection of Cyanide in Aqueous Solution Based on the Aggregation-Induced Emission. *Org. Lett.* **2009**, *11*, 1943−1946.
(19) Wei, S. C.; Hsu, P. H.; Lee, Y. F.; Lin, Y. W.; Huang, C. C. Selective Detection of Iodide and Cyanide Anions Using Gold-Nanoparticle-Based Fluorescent Probes. *ACS Appl. Mater. Interfaces* **2012**, *4*, 2652−2658.
(20) Bhalla, V.; Pramanik, S.; Kumar, M. Cyanide Modulated Fluorescent Supramolecular Assembly of a Hexaphenylbenzene Derivative for Detection of Trinitrotoluene at the Attogram Level. *Chem. Commun.* **2013**, *49*, 895−897.
(21) Saha, S.; Ghosh, A.; Mahato, P.; Mishra, S.; Mishra, S. K.; Suresh, E.; Das, S.; Das, A. Specific Recognition and Sensing of CN^- in Sodium Cyanide Solution. *Org. Lett.* **2010**, *12*, 3406−3409.
(22) Ekmekci, Z.; Yilmaz, M. D.; Akkaya, E. U. A Monostyryl-Boradiazaindacene (BODIPY) Derivative as Colorimetric and Fluorescent Probe for Cyanide Ions. *Org. Lett.* **2008**, *10*, 461−464.
(23) Lin, Q.; Liu, X.; Wei, T. B.; Zhang, Y. M. Reaction-Based Ratiometric Chemosensor for Instant Detection of Cyanide in Water with High Selectivity and Sensitivity. *Chem.—Asian J.* **2013**, *8*, 3015−3021.
(24) Jo, J.; Olasz, A.; Chen, C. H.; Lee, D. Interdigitated Hydrogen Bonds: Electrophile Activation for Covalent Capture and Fluorescence Turn-On Detection of Cyanide. *J. Am. Chem. Soc.* **2013**, *135*, 3620−3632.
(25) Yang, L.; Li, X.; Yang, J.; Qu, Y.; Hua, J. Colorimetric and Ratiometric Near-Infrared Fluorescent Cyanide Chemodosimeter Based on Phenazine Derivatives. *ACS Appl. Mater. Interfaces* **2013**, *5*, 1317−1326.
(26) Lin, Y. D.; Pen, Y. S.; Su, W. T.; Liau, K. L.; Wen, Y. S.; Tu, C. H.; Sun, C. H.; Chow, T. J. Reaction-Based Colorimetric and Ratiometric Fluorescence Sensor for Detection of Cyanide in Aqueous Media. *Chem.—Asian J.* **2012**, *7*, 2864−2871.
(27) Chung, S. Y.; Nam, S. W.; Lim, J.; Park, S.; Yoon, J. A Highly Selective Cyanide Sensing in Water via Fluorescence Change and Its Application to in Vivo Imaging. *Chem. Commun.* **2009**, 2866−2868.
(28) Lou, X.; Qiang, L.; Qin, J.; Li, Z. A New Rhodamine-Based Colorimetric Cyanide Chemosensor: Convenient Detecting Procedure and High Sensitivity and Selectivity. *ACS Appl. Mater. Interfaces* **2009**, *1*, 2529−2535.
(29) Bhalla, V.; Singh, H.; Kumar, M. Triphenylene Based Copper Ensemble for the Detection of Cyanide ions. *Dalton Trans.* **2012**, *41*, 11413−11418.
(30) Peng, X.; Wu, Y.; Fan, J.; Tian, M.; Han, K. Colorimetric and Ratiometric Fluorescence Sensing of Fluoride: Tuning Selectivity in Proton Transfer. *J. Org. Chem.* **2005**, *70*, 10524−10531.
(31) Liu, B.; Tian, H. A Ratiometric Fluorescent Chemosensor for Fluoride Ions Based on a Proton Transfer Signaling Mechanism. *J. Mater. Chem.* **2005**, *15*, 2681−2686.
(32) Kubo, Y.; Yamamoto, M.; Ikeda, M.; Takeuchi, M.; Shinkai, S.; Yamaguchi, S.; Tamao, K. A Colorimetric and Ratiometric Fluorescent Chemosensor with Three Emission Changes: Fluoride Ion Sensing by

a Triarylborane−Porphyrin Conjugate. *Angew. Chem., Int. Ed.* **2003**, *42*, 2036−2040.
(33) Xu, Z.; Chen, W. X.; Kim, W. H. N.; Yoon, J. Sensors for the Optical Detection of Cyanide Ion. *Chem. Soc. Rev.* **2010**, *39*, 127−137.
(34) Liu, Y.; Lv, X.; Zhao, Y.; Liu, J.; Sun, Y. Q.; Wang, P.; Guo, W. A Cu(II)-Based Chemosensing Ensemble Bearing Rhodamine B Fluorophore for Fluorescence Turn-On Detection of Cyanide. *J. Mater. Chem.* **2012**, *22*, 1747−1750.
(35) Magnusson, R.; Nyholm, S.; Åstot, C. Analysis of Hydrogen Cyanide in Air in a Case of Attempted Cyanide Poisoning. *Forensic Sci. Int.* **2012**, *222*, e7−e12.
(36) Cheng, X.; Zhou, Y.; Qin, J.; Li, Z. Reaction-Based Colorimetric Cyanide Chemosensors: Rapid Naked-Eye Detection and High Selectivity. *ACS Appl. Mater. Interfaces* **2012**, *4*, 2133−2138.
(37) Cheng, X.; Tang, R.; Jia, H.; Feng, J.; Qin, J.; Li, Z. New Fluorescent and Colorimetric Probe for Cyanide: Direct Reactivity, High Selectivity and Bioimaging Application. *ACS Appl. Mater. Interfaces* **2012**, *4*, 4387−4392.
(38) Martinez-Manez, R.; Sancenon, F. Fluorogenic and Chromogenic Chemosensors and Reagents for Anions. *Chem. Rev.* **2003**, *103*, 4419−4476 and references therein.
(39) Brooks, S. J.; Gale, P. A.; Light, M. E. Carboxylate Complexation by 1,1′-(1,2-Phenylene)bis(3-phenylurea) in Solution and the Solid State. *Chem. Commun.* **2005**, 4696−4698.
(40) Ajayaghosh, A.; Carol, P.; Sreejith, S. A Ratiometric Fluorescence Probe for Selective Visual Sensing of Zn^{2+}. *J. Am. Chem. Soc.* **2005**, *127*, 14962−14963.
(41) Goswami, S.; Manna, A.; Paul, S.; Das, A. K.; Aich, K.; Nandi, P. K. Resonance-Assisted Hydrogen Bonding Induced Nucleophilic Addition to Hamper ESIPT: Ratiometric Detection of Cyanide in Aqueous Media. *Chem. Commun.* **2013**, *49*, 2912−2914.
(42) Kumar, M.; Reja, S. I.; Bhalla, V. A Charge Transfer Amplified Fluorescent Hg^{2+} Complex for Detection of Picric Acid and Construction of Logic Functions. *Org. Lett.* **2012**, *14*, 6084−6087.
(43) Kumar, M.; Kumar, R.; Bhalla, V. Fluorescent Probe for Fe^{3+} and CN^- in Aqueous Media Mimicking a Memorized Molecular Crossword Puzzle. *RSC Adv.* **2011**, *1*, 1045−1049.
(44) Pramanik, S.; Bhalla, V.; Kumar, M. Mercury Assisted Fluorescent Supramolecular Assembly of Hexaphenylbenzene Derivative for Femtogram Detection of Picric Acid. *Anal. Chim. Acta* **2013**, *793*, 99−106.
(45) Bhalla, V.; Vij, V.; Dhir, A.; Kumar, M. Hetero-Oligophenylene-Based AIEE Material as a Multiple Probe for Biomolecules and Metal Ions to Construct Logic Circuits: Application in Bioelectronics and Chemionics. *Chem.—Eur. J.* **2012**, *18*, 3765−3772.
(46) Chen, C. L.; Chen, Y. H.; Chen, C. Y.; Sun, S. S. Dipyrrole Carboxamide Derived Selective Ratiometric Probes for Cyanide Ion. *Org. Lett.* **2006**, *8*, 5053−5056.
(47) Hong, Y.; Lam, J. W. Y.; Tang, B. Z. Aggregation-Induced Emission. *Chem. Soc. Rev.* **2011**, *40*, 5361−5388.
(48) Shi, C.; Guo, Z.; Yan, Y.; Zhu, S.; Xie, Y.; Zhao, Y. S.; Zhu, W.; Tian, H. Self-Assembly Solid-State Enhanced Red Emission of Quinolinemalononitrile: Optical Waveguides and Stimuli Response. *ACS Appl. Mater. Interfaces* **2013**, *5*, 192−198.
(49) Shao, A.; Guo, Z.; Zhu, S.; Zhu, S.; Shi, P.; Tian, H.; Zhu, W. Insight Into Aggregation-Induced Emission Characteristics of Red-Emissive Quinolinemalononitrile by Cell Tracking and Real-Time Trypsin Detection. *Chem. Sci.* **2014**, *5*, 1383−1389.
(50) Compound **3** is better in comparison to CN^- sensors reported in the literature. For comparison with reported cyanide sensors, please see the Supporting Information Figure S25 (Table 1).
(51) Bhalla, V.; Roopa; Kumar, M. A Pentaquinone Based Probe for Relay Recognition of F^- and Cu^{2+} Ions: Sequential Logic Operations at the Molecular Level. *Dalton Trans.* **2013**, *42*, 13390−13396.
(52) Yao, J.; Zhang, K.; Zhu, H.; Ma, F.; Sun, M.; Yu, H.; Sun, J.; Wang, S. Efficient Ratiometric Fluorescence Probe Based on Dual-Emission Quantum Dots Hybrid for On-Site Determination of Copper Ions. *Anal. Chem.* **2013**, *85*, 6461−6468.
(53) Long, G. L.; Winefordner, J. D. The Limit of Detection is the Lowest Concentration Level That Can Be Determined To Be Statistically Different from an Analytical Blank. Significant Problems Have Been Encountered in Expressing These Values Because of the Various Approaches to the Term "Statistically Different". *Anal. Chem.* **1983**, *55*, 712A−723A.
(54) Badugu, R.; Lakowicz, J. R.; Geddes, C. D. Enhanced Fluorescence Cyanide Detection at Physiologically Lethal Levels: Reduced ICT-Based Signal Transduction. *J. Am. Chem. Soc.* **2005**, *127*, 3635−3641.
(55) Sun, S. S.; Lees, A. J.; Zavalij, P. Y. Highly Sensitive Luminescent Metal-Complex Receptors for Anions through Charge-Assisted Amide Hydrogen Bonding. *Inorg. Chem.* **2003**, *42*, 3445−3453.
(56) Thiagarajan, V.; Ramamurthy, P.; Thirumalai, D.; Ramakrishnan, V. T. A Novel Colorimetric and Fluorescent Chemosensor for Anions Involving PET and ICT Pathways. *Org. Lett.* **2005**, *7*, 657−660.
(57) Xia, H.; Liu, D.; Song, K.; Miao, Q. Vapochromic and Semiconducting Solids of a Bifunctional Hydrocarbon. *Chem. Sci.* **2011**, *2*, 2402−2406.
(58) McGuire, R. J.; Dogutan, D. K.; Teets, T. S.; Suntivich, J.; Horn, Y. S.; Nocera, D. G. Oxygen Reduction Reactivity of Cobalt(II) Hangman Porphyrins. *Chem. Sci.* **2010**, *1*, 411−414.
(59) Cao, Q. Y.; Pradhan, T.; Kim, S.; Kim, J. S. Ferrocene-Appended Aryl Triazole for Electrochemical Recognition of Phosphate Ions. *Org. Lett.* **2011**, *13*, 4386−4389.
(60) Chung, Y. M.; Raman, B.; Kim, D. S.; Ahn, K. H. Fluorescence Modulation in Anion Sensing by Introducing Intramolecular H-Bonding Interactions in Host−Guest Adducts. *Chem. Commun.* **2006**, 186−188.
(61) Hsu, H. F.; Lin, M. C.; Lin, W. C.; Lai, Y. H.; Lin, S. Y. Novel Columnar Liquid Crystals with Nonidentical Peripheral Groups: 1,3,5-Triphenylethynyl-2,4,6-triphenylbenzene. *Chem. Mater.* **2003**, *15*, 2115−2118.
(62) Garc, L. J.; Kaltbeitzel, A.; Pisula, W.; Gutmann, J. S.; Klapper, M.; Mullen, K. Phosphonated Hexaphenylbenzene: A Crystalline Proton Conductor. *Angew. Chem., Int. Ed.* **2009**, *48*, 9951−9953.
(63) Edelsztein, V. C.; Cormack, A. S. M.; Ciarlantini, M.; Chenna, P. H. D. Self-Assembly of 2,3-Dihydroxycholestane Steroids into Supramolecular Organogels as a Soft Template for the in-Situ Generation of Silicate Nanomaterials. *Beilstein J. Org. Chem.* **2013**, *9*, 1826−1836.
(64) Roll, M. F.; Kampf, J. W.; Laine, R. M. Crystalline Hybrid Polyphenylene Macromolecules from Octaalkynylsilsesquioxanes, Crystal Structures, and a Potential Route to 3-D Graphenes. *Macromolecules* **2011**, *44*, 3425−3435.
(65) Sun, H.; Mei, H.; An, G.; Han, J.; Pan, Y. Hydrogen-Bonding Self-Assembly of Two Dimensional (2D) Layer Structures Generating Metal−Organic Nanotubes. *CrystEngComm* **2011**, *13*, 734−737.
(66) Jang, S.; Kim, S. G.; Jung, D.; Kwon, H.; Song, J.; Cho, S.; Ko, Y. C.; Sohn, H. Aggregation-Induced Emission Enhancement of Polysilole Nanoaggregates. *Bull. Korean Chem. Soc.* **2006**, *27*, 1965−1966.
(67) Kartha, K. K.; Babu, S. S.; Srinivasan, S.; Ajayaghosh, A. Attogram Sensing of Trinitrotoluene with a Self-Assembled Molecular Gelator. *J. Am. Chem. Soc.* **2012**, *134*, 4834−4841.
(68) Szacilowski, K. Digital Information Processing in Molecular Systems. *Chem. Rev.* **2008**, *108*, 3481−3548.
(69) de Silva, A. P.; McClenaghan, N. D. Molecular-Scale Logic Gates. *Chem.—Eur. J.* **2004**, *10*, 574−586.
(70) Kumar, M.; Kumar, N.; Bhalla, V. A Naphthalimide Based Chemosensor for Zn^{2+}, Pyrophosphate and H_2O_2: Sequential Logic Operations at the Molecular Level. *Chem. Commun.* **2013**, *49*, 877.